Applied Catalysis B: Environmental 87 (2009) 37–45

Contents lists available at ScienceDirect

Applied Catalysis B: Environmental

journal homepage: www.elsevier.com/locate/apcatb

MTW zeolites for reducing cold-start emissions of automotive exhaust

Z. Sarshar [a], M.H. Zahedi-Niaki [a], Q. Huang [b], M. Eić [b], S. Kaliaguine [a,*]

[a] Department of Chemical Engineering, Université Laval, Québec, Canada, G1K 7P4
[b] Department of Chemical Engineering, University of New Brunswick, Fredericton, N.B., Canada, E3B 5A3

ARTICLE INFO

Article history:
Received 27 June 2008
Received in revised form 12 August 2008
Accepted 21 August 2008
Available online 3 September 2008

Keywords:
Hydrocarbon trap
ZSM-12
Ion-exchange
Isomorphous substitution
Cold-start emissions
Temperature-programmed desorption
Single-file diffusion
Adsorption

ABSTRACT

Increasingly strict environmental legislations have led to the need for better control of vehicle cold-start emissions. In this research work, a series of one-dimensional channel molecular sieves with 12 oxygen ring apertures (12R) having MTW structure (MTW is the designation for ZSM-12 in the IZA nomenclature of zeolite structures), have been synthesized and characterized by different techniques such as: XRD, SEM, BET surface area, elemental analysis by atomic absorption spectroscopy, FTIR of adsorbed pyridine and temperature-programmed desorption (TPD). The synthesized samples were tested as hydrocarbons (HCs) trap adsorbents using toluene and ethylene as heavy (aromatic) and light (olefin) probe molecules present in the exhaust stream at engine cold-start. TPD tests were performed after adsorption under four different mixture conditions: binary (toluene–ethylene), ternary (toluene–ethylene–CO_2), ternary (toluene–ethylene–H_2O) and quaternary (toluene–ethylene–CO_2–H_2O). The results demonstrated that a silver exchanged MTW zeolite, Al-ZSM-12 (Ag) exhibited high and stable trapping capacities for both probe molecules in all mixtures investigated in this study, thus showing essentially no sensitivity to CO_2 and/or H_2O. Moreover, a high desorption temperature, particularly for toluene, was associated with the large amount of strong Lewis and Brönsted acid sites. Isomorphous substitution of Al by Fe in MTW structures did not lead to drastic changes in adsorption capacities and desorption temperatures of the two sorbates.

1. Introduction

Over the recent years, the low emission standards have forced automobile and catalyst manufacturers to focus on reducing the cold-start hydrocarbons (“HCs”) emissions. Cold-start is referring to the short time period of 1–2 min, after engine ignition, before the three-way catalyst reaches its light-off temperature. During this period about 70–80% of the total hydrocarbons are released without converting due to sluggish catalyst activity at low temperature. Different approaches have been attempted to solve this problem including combustion heated catalyst (CHC) [1], electrically heated catalyst [2–5], close-coupled catalyst [6,7], exhaust-gas ignition (EGI) [8,9] and heat storage devices but all these solutions encountered difficulties such as: cost, complexity in design and fabrication and durability. It has been found that the effective solution to the cold-start problem is to design a system employing an adsorbent which traps the hydrocarbons temporarily, followed by their gradual desorption from the porous structure upon increasing exhaust temperature. For this solution, zeolites have been found preferred adsorbent materials due to their thermal stability and their thermodynamic affinity to HCs. The critical factors for any emission trap are the adsorption capacity and desorption temperature which must be higher than the catalyst light-off temperature [10].

A series of zeolites BEA, MFI, MOR and X [11–13] and silicoaluminophosphate molecular sieves [14] were investigated regarding their hydrocarbon adsorption capacities, under a variety of conditions [15]. Bruke et al. [16] reported that beta zeolite (BEA) is a promising material for this application, while Elangovan et al. [17] found that Standard Oil Synthetic Zeolite-thirty-three (SSZ-33) is superior to BEA based on their adsorption studies of a series of medium and large pore silicoaluminate zeolites. On the other hand, Czaplewski et al. [18] observed an interesting phenomenon of trapping molecules within the one-dimensional channel of EUO and MOR zeolites, as compared to more typical three-dimensional zeolites. This phenomenon was designated as the single-file diffusion mechanism, which prevents the passage of molecules by one another inside the micropores of the one-dimensional zeolites.

In a previous work we have studied a number of one-dimensional zeolites which could potentially be employed as adsorbents for HC traps during cold-start. ZSM-12 was selected as a promising candidate from these preliminary screening tests, based on its high

* Corresponding author.
E-mail address: Serge.Kaliaguine@gch.ulaval.ca (S. Kaliaguine).

0926-3373/$ – see front matter © 2008 Elsevier B.V. All rights reserved.
doi:10.1016/j.apcatb.2008.08.025

trapping capacity and desorption temperature [19,22]. In particular ZSM-12 was found to be hydrothermally stable up to 973–1073 K in the presence of 10% water vapour in helium [22]. In the present study, the influence of isomorphous metal substitutions, cation exchange and acid properties of synthesized ZSM-12 (MTW) samples on trapping capacities and desorption temperatures of both probe molecules were investigated.

2. Experimental details

2.1. Al-ZSM-12 synthesis

Al-ZSM-12 was synthesized using a method proposed by Ernst et al. [20]. In a typical preparation, 80.9 g of a sodium silicate solution (Merck, 28.5 wt.% SiO_2, 8.8 wt.% Na_2O, 62.7 wt.% H_2O) was mixed with 80 g distilled water. To this, a solution of 30 g methyltriethylammoniumchloride (Fluka) in 100 g water was added, under stirring, followed by adding a solution containing 2.4 g $Al(NO_3)_3{\cdot}9H_2O$ (Merck) in 30 g H_2O. Afterwards, 4.7 g H_2SO_4 (Merck, 98%) was added under vigorous stirring. In the next step, the gel was transferred into a Teflon-lined stainless steel autoclave and the crystallization was conducted in a furnace at 433 K without agitation for 7 days. The final products were separated by centrifugation and then repeatedly washed with distilled water, followed by drying in air at 343 K overnight. Finally, calcination at 823 K was carried out overnight. The molar composition of the resulting gel was calculated as $SiO_2/Al_2O_3 = 120$, $OH^-/SiO_2 = 0.3$, $Na_2O/(MTEA)_2O = 1.5$ and $H_2O/OH^- = 125$.

2.2. Ion exchange of ZSM-12

The calcined zeolites were three-fold ion-exchanged at room temperature with 0.1 M ammonium nitrate solution. Ag incorporation was carried out by ion-exchange in the liquid phase using silver nitrate over H-form of zeolite samples. For this, the solution was stirred at 353 K for 2 h. Thereafter, the samples were centrifuged and washed with distilled water and then dried overnight at 373 K.

2.3. Fe-ZSM-12 synthesis

The hydrothermal synthesis of Fe-ZSM-12 was carried out by modifying the procedure reported by Ernst et al. for the synthesis of ZSM-12. In a typical preparation of Fe-ZSM-12 [21], a required amount of sodium silicate (27.8 wt.% SiO_2, 8.8 wt.% Na_2O and 63.4 wt.% H_2O) in 40 g H_2O was added slowly under stirring to another solution comprising specified amount of $Fe(NO_3)_3{\cdot}9H_2O$, 40 g H_2O and 3.0–4.0 g H_2SO_4 (96–98 wt.%). To the above mixture adequate amount of methyltriethylammoniumchloride (MTEA-Cl, Fluka) in 40 g H_2O was added under vigorous stirring. The pale lemon-coloured gel, so obtained, was stirred for about half an hour before transferring into a Teflon-lined stainless steel autoclave. The typical molar gel composition was: $SiO_2/Fe_2O_3 = 140$, $SiO_2/MTEA^+ = 2.5$, $SiO_2/Na^+ = 1.67$, $OH^-/SiO_2 = 0.214$ and $H_2O/SiO_2 = 47$. The crystallization was carried out at 433 K for 5 days. The colour of the crystalline product was white. The final products were separated by centrifugation and then repeatedly washed with distilled water, followed by drying in air at 343 K overnight. Thereafter, calcination was carried out at 873 K overnight. The gel compositions of the different samples are presented in Table 1.

3. Structural characterization

3.1. XRD

In X-ray diffraction (XRD) patterns the unique structures of the different zeolites, in terms of atom positions and unit cell dimensions, are reflected in characteristic positions and relative intensities of observed peaks. Powder X-ray diffraction patterns of the as-synthesized and calcined samples were recorded using a Siemens D5000 powder diffractometer with Cu Kα radiation (λ = 1.54184 Å).

3.2. SEM

Scanning electron micrographs were recorded to determine the crystallite size and characterize the morphology of the materials, using a JEOL JSM-840A SEM operated at 15–20 kV.

3.3. Elemental analysis

The bulk chemical compositions of the samples were determined by elemental analysis. The bulk composition of the calcined samples (practically Si/M atomic ratio = y/x) was determined by the so-called wet analysis method. A complete acid digestion prior to analysis by inductively coupled plasma–atomic emission spectroscopy (ICP–AES) or flame atomic absorption spectroscopy (AAS) was required. The AAS analysis was carried out using a PerkinElmer 1100B atomic absorption spectrometer. The ICP analyses were carried out using a P40 spectrometer also from PerkinElmer.

3.4. Nitrogen adsorption

The sorption isotherms of nitrogen measured at its condensation temperature (77 K) reflect the textural characteristics of the materials. In this work, the nitrogen adsorption measurements were performed to characterize the textural properties of the calcined samples, including the total BET surface area and the micropore volume.

The adsorption and/or desorption isotherms of nitrogen at 77 K were obtained using an Omnisorp-100 automatic analyzer after degassing the calcined samples at 573 K for at least 4 h under vacuum 0.013–0.0013 Pa. The linear part of the Brunauer–

Table 1
Gel composition of synthesized samples

Sample	Acronym	Si/Al	Si/Fe	Gel composition*				
				r	x	y	z	m
ZS1-29	Al-ZSM-12	60		1.0	0.016	0.000	1.89	226.13
ZS1-26	Fe-ZSM-12		40	1.0	0.000	0.030	2.39	122.10
ZS1-36	Fe-ZSM-12		50	1.0	0.000	0.024	2.39	122.10
ZS1-24	Fe-ZSM-12		70	1.0	0.000	0.017	2.39	122.10
ZS1-28	Al-Fe-ZSM-12	40	40	1.0	0.014	0.014	2.39	122.10
ZS1-32	Al-Fe-ZSM-12	60	60	1.0	0.010	0.010	2.39	122.10

* rR:xAl$_2$O$_3$:yFe$_2$O$_3$:zSiO$_2$:mH$_2$O; R = MTEA-Cl.

Emmett–Teller (BET) equation (P/P^0 = 0.06–0.10) was used to calculate specific surface area. The *t*-plot method was applied to quantitatively determine the micropore volumes of zeolites.

3.5. Fourier transform infrared spectroscopy (FTIR)

FTIR coupled with adsorption of basic probe molecules like pyridine yields information concerning the nature of acid sites (Brönsted and Lewis), while the FTIR spectra after adsorption at different temperatures provide information about the acid strength. FTIR of adsorbed pyridine was performed using a Biorad FTS-60 spectrometer. About 8 mg wafers of calcined samples were first evacuated (0.013 Pa) at 573 K for 24 h. The spectra were then recorded at room temperature. The samples were then exposed to 2373.1 Pa of pyridine vapour at 297 K for 10 min. In each step of pyridine desorption, the samples were evacuated (0.013 Pa) at different temperatures (373, 423,473, 573 and 673 K) for 12 h before the spectra were recorded at room temperature in the evacuated cell.

3.6. Ammonia thermodesorption (TPD of adsorbed ammonia)

Ammonia thermodesorption profiles were obtained using a RXM-100 catalyst characterization system (ASDI) equipped with an online mass spectrometer (UTI 100) and a thermal conductivity detector (TCD). About 0.1 g of calcined sample was placed in a U-shaped quartz reactor between two plugs of quartz wool. The sample was then pretreated at 823 K under a flow of 20% oxygen in helium and cooled down to room temperature under the same flowing gas. The reactor was then heated to 373 K and pure ammonia was admitted to the reactor (1 atm) for 15 min. Physisorbed NH_3 was removed by purging with helium. Heating was then carried out at a rate of 5 K/min until 823 K, under the same gas flow. Quantification of the response peaks was obtained after calibration of the TCD response curves.

3.7. Temperature-programmed desorption

Temperature-programmed desorption (TPD) was carried out in a custom-made flow device with helium as a carrier gas. Toluene and ethylene were used as probe molecules for heavy and light components of automobile exhaust gases, respectively. For each experiment 10 mg of the sample was placed between two sintered discs in a 0.14 in I.D. stainless steel tube. Subsequently, activation of the sample was carried out in a flow of helium at 573 K for 2 h and then cooled down to a temperature of 303 K. After this procedure, adsorption of the probe molecules was performed by introducing the sorbates diluted with helium at 303 K (50 cm^3 STP/min) for a period of 15 min. The partial pressures of toluene and ethylene during the adsorption step were kept constant at 0.25 kPa. The gas phase and the weakly adsorbed sorbates on the surface of crystals were purged with pure helium at 303 K for 15 min.

Desorption was then performed by heating the sample in the flow of helium from 303 to 623 K at a linear heating rate of 20 K/min. After the final temperature was reached, desorption was continued for a further period of 10 min to desorb any residual sorbate. Helium flow rate was maintained at 50 cm^3 (STP)/min. The effluent gas stream during TPD was continuously monitored using a quadrupole mass spectrometer (Dycor Dymaxion Quadrupole MS).

4. Results and discussions

4.1. XRD

Selected XRD patterns of calcined samples are shown in Fig. 1. These patterns confirm that the samples are pure with the MTW crystal structure. The high intensity of the XRD lines indicates that the samples are well crystalline materials.

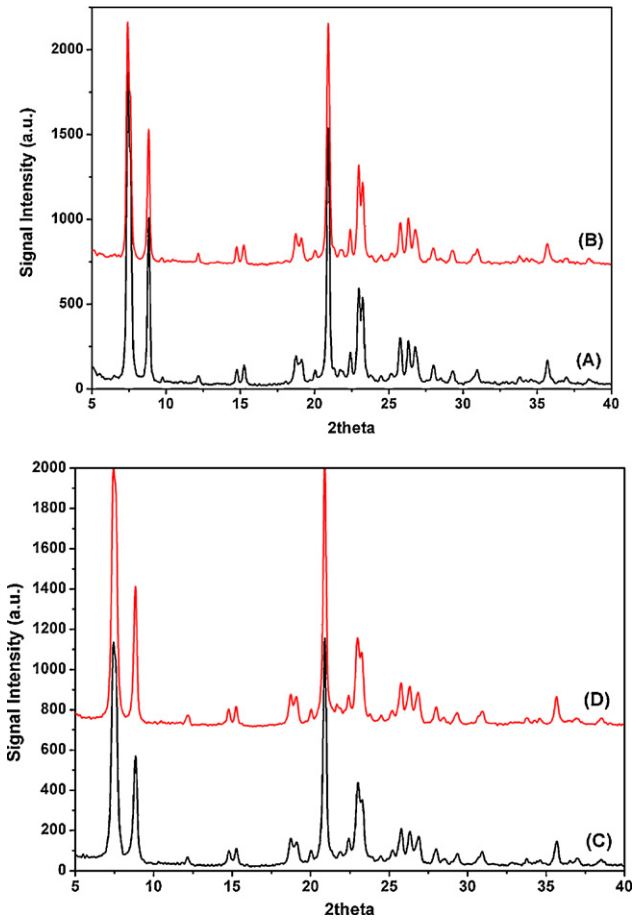

Fig. 1. XRD of selected as-synthesized samples. (A) Al-ZSM-12 (Na); (B) Al-ZSM-12 (H); (C) Fe-ZSM-12 (40); (D) Al-Fe-ZSM-12 (40).

4.2. SEM

The SEM images of some selected samples are displayed in Fig. 2. The individual crystals of Na-ZSM-12 (Fig. 2A) appear to be rice-shaped with average crystal diameter of 2.7 μm, while Iliyas et al. [22] reported the spherical shape crystallite because of using tetraethylammonium hydroxide (TEAOH) as the structure directing agent. Isomorphous substitution of Al by Fe results in changing the morphology to the spherical shape or hank-shaped crystallites (Fig. 2B), as well as appearance of some plate-shaped crystallites (Fig. 2C). Fig. 2A and B shows that the particles are agglomerates of very small crystals (a fraction of micron in size). On the other hand Na-ZSM-12 particles (Fig. 2A) look much more homogeneous.

4.3. Elemental analysis

The results of bulk composition analyses are summarized in Table 2. From this table, it can be found that comparable bulk phase chemical compositions are observed for the solid products and the corresponding gel phases.

Moreover, the degree of ion exchange of calcined Na-ZSM-12 for H^+, Ag^+ and Mg^{2+} cations in samples ZS1-29-1, 29-2 and 29-3 were found to be 0.78, 0.96 and 0.65, respectively.

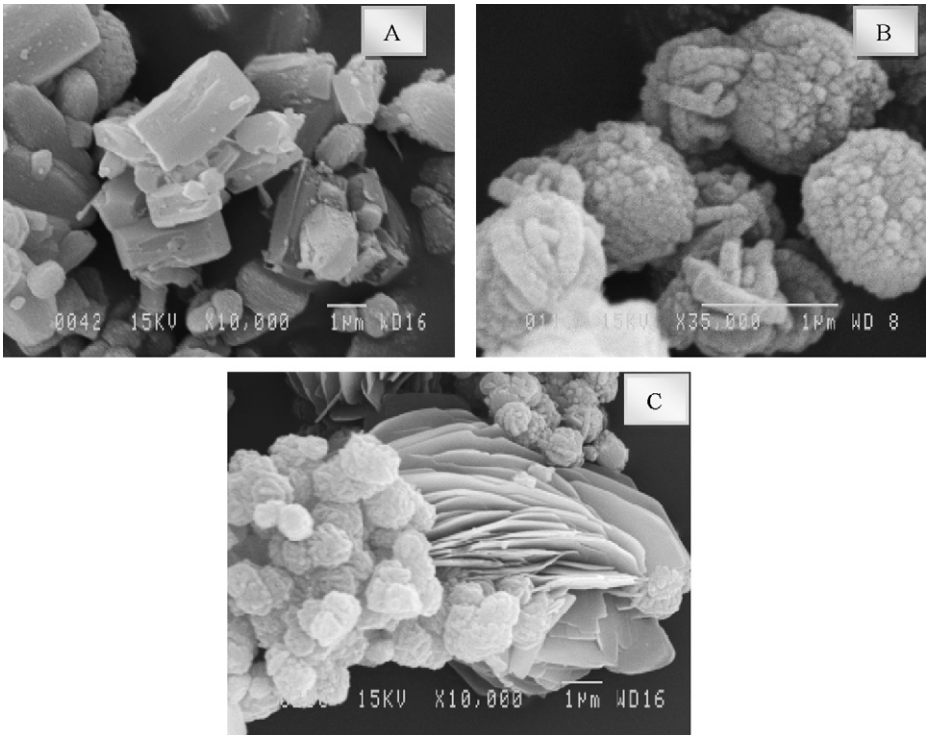

Fig. 2. SEM pictures of selected as-synthesized samples. (A) Na-ZSM-12; (B) Fe-ZSM-12 (40); (C) Fe-ZSM-12 (70).

4.4. Nitrogen adsorption

The measured values of specific surface area and micropore volume of the samples are shown in Table 3. They reveal that Al-ZSM-12 samples in all cationic forms (except exchanged with Mg^{2+}) possess high surface area (close to 300 m^2/g) and micropore volume (above 0.12 cm^3/g), which are desirable properties related to sorbates adsorption capacity. Substituting Al^{3+} with Fe^{3+} leads to lower surface area and/or micropore volume probably due to extra-framework oxide clusters that can create pore clogging in zeolites and reduce the pore volume available for nitrogen adsorption. The higher the content of extra-framework Fe^{3+}, the lower the surface area and micropore volume.

4.5. Fourier transform infrared spectroscopy

In this characterization technique, Brönsted acid centres are detected by a band around 1548 cm^{-1}, which originates from pyridinium ions ($C_5H_5NH^+$) created via protonation of pyridine molecules by surface acidic hydroxyl groups [23]. On the other hand, Lewis acidic centres are characterized by bands around 1450 cm^{-1}, originating from pyridine coordinatively linked to Lewis acidic sites. However, bands of physisorbed pyridine are expected in the range close to Lewis acidic centres, i.e., around 1443 cm^{-1}. These additional bands may be removed at higher desorption temperature, e.g., above 423 K. The measured amounts of both acid sites decreased as pyridine desorption temperature increased and finally no pyridine desorbing from acidic sites was observed at 673 K for all samples.

The concentration ratios of Brönsted to Lewis acid sites for all samples are presented in Table 4. H-ZSM-12 has the highest measured $C_{Brönsted}/C_{Lewis}$ and this ratio decreases in the order of: $H^+ > Na^+ > Mg^{2+} > Ag^+$. Ag-ZSM-12 has the largest amount of Lewis acid sites (the lowest ratio) in comparison to the other samples. The Fe-ZSM-12 sample with Si/Fe = 40 also has a high Lewis acid site content. The 1448 cm^{-1} peak area, related to Lewis sites, decreases with increasing Si/Fe ratio in the Fe substituted samples, whereas $C_{Brönsted}/C_{Lewis}$ ratio increases. Consequently, the higher the Si/Fe ratio in Fe-ZSM-12 samples, the higher the ratio $C_{Brönsted}/C_{Lewis}$. This ratio is increased by partial substitution of Fe by Al into the framework. For instance in the case of Al-Fe-ZSM-12 (40), this ratio is 2.9, whereas for Fe-ZSM-12 (40) it is 1.9. Thus, the Si/M ratio (M is a trivalent element), the nature of the trivalent element and the type of counter-cation are the most important factors that influence the nature and quantity of the acid sites which in turn control the adsorption/desorption behaviour of the zeolites. Typical chemisorbed pyridine FTIR spectra of Na-ZSM-12 and Ag-ZSM-12 at different desorption temperatures are shown in Fig. 3.

Table 2
Results of bulk chemical composition of calcined samples by AAS

Sample	Trivalent element (M)	Si/M[a]	Si/M[b]
ZS1-29	Al	79	60
ZS1-28	Al, Fe	40[c]	40[c]
ZS1-28	Al, Fe	47[d]	40[d]
ZS1-32	Al, Fe	62[c]	60[c]
ZS1-32	Al, Fe	55[d]	60[d]
ZS1-24	Fe	68	70
ZS1-36	Fe	49	50
ZS1-26	Fe	45	40

[a] Ratio in solid product.
[b] Ratio in the gel.
[c] M = Al.
[d] M = Fe.

4.6. Ammonia thermodesorption (TPD of adsorbed ammonia)

The TPD results of adsorbed ammonia of all ZSM-12 samples are shown in Table 5, while a typical NH_3-TPD profile of Ag-ZSM-12 sample is shown in Fig. 4. Three distinct regions are observed in the TPD profiles. These peaks can be designated as 1, 2 and 3 and

Table 3
Textural properties from nitrogen adsorption isotherms at 77 K

Sample*	Trivalent element	Si/M	Ionic form	Surface area (m^2/g)	Micropore volume (ml/g)
ZS1-29	Al	60	Na^+	342	0.131
ZS1-29-1	Al	60	H^+	324	0.123
ZS1-29-2	Al	60	Ag^+	293	0.122
ZS1-29-3	Al	60	Mg^+	257	0.099
ZS1-26	Fe	40	Na^+	283	0.120
ZS1-36	Fe	50	Na^+	290	0.122
ZS1-24	Fe	70	Na^+	311	0.123
ZS1-28	Al, Fe	40	Na^+	339	0.128
ZS1-32	Al, Fe	60	Na^+	235	0.101

Specific surface area values are ±5 m^2/g whereas micropore volumes are ±0.001 ml/g.
* All samples have MTW structure.

Table 4
FTIR results of chemisorbed pyridine (desorption at 423 K)

Sample	Peak area (a.u.) 1448 cm^{-1}	Peak area (a.u.) 1550 cm^{-1}	$C_{Brönsted}/C_{Lewis}$*
Na-ZSM-12	0.010	0.347	45.9
H-ZSM-12	0.012	0.732	80.8
Ag-ZSM-12	0.471	0.183	0.5
Mg-ZSM-12	0.120	0.220	2.4
Fe-ZSM-12 (40)	0.272	0.398	1.9
Fe-ZSM-12 (50)	0.213	0.521	3.2
Fe-ZSM-12 (70)	0.078	0.335	5.7
Al-Fe-ZSM-12 (40)	0.228	0.498	2.9
Al-Fe-ZSM-12 (60)	0.107	0.403	5.0

* Calculated as $A_{1550} \times 1.88/A_{1448} \times 1.42$.

correspond to weak, medium and strong acid centres in zeolites, respectively.

It is also seen from this table that the amount of adsorbed ammonia in the low temperature region of the desorption profile, which can be assigned to Lewis acid sites, increases in the order: $Ag^+ > H^+ > Mg^{2+} > Na^+$ for Al-ZSM-12 and Si/Fe = 40 > 50 > 70 for Fe-ZSM-12 samples. In fact, Ag-ZSM-12 and Fe-ZSM-12 (40) have the largest amounts of Lewis acid sites among the Al and Fe samples, respectively. The amount of adsorbed ammonia in the medium temperature region of desorption profile can be assigned either to Lewis or Brönsted acid sites, depending on the samples. Finally, the amount of adsorbed ammonia in the high temperature region of the profile, which may be attributed to strong Brönsted acid sites, increases in the order: $H^+ > Na^+ > Ag^+ > Mg^{2+}$. It can also be seen that by increasing the Si/Fe ratio for Fe-ZSM-12 samples, the amount of these strong acid sites increases.

Comparing these peak temperatures in the three distinct regions can lead to a clear assessment regarding the acid strength of the sites. Generally, it can be seen that the ammonia desorption temperatures (from NH_3-TPD profiles) are higher for Al-ZSM-12 samples than for Fe-ZSM-12 samples. This corresponds to the fact that Al as a trivalent element in the framework of zeolites can generate stronger acid sites than Fe. Among Al-ZSM-12 samples, the one having Ag counter-ions shows the highest desorption temperature in the low temperature region (200 °C) and thus stronger Lewis acid sites compared to Na^+ cations. The strongest Brönsted acid sites correspond to NH_3 desorbing from proton sites in Na-ZSM-12 and H-ZSM-12 at 395 and 380 °C, respectively.

All the above conclusions are confirmed by the FTIR of chemisorbed pyridine. Comparing the NH_3-TPD for Fe-ZSM-12 samples indicates a systematic decrease in the amounts of NH_3 desorbed at the lowest temperature (T_{peak1}) as the Si/Fe ratio increases. At the same time the amounts of ammonia desorbed as both the other two peaks (peaks 2 and 3) increase. This would

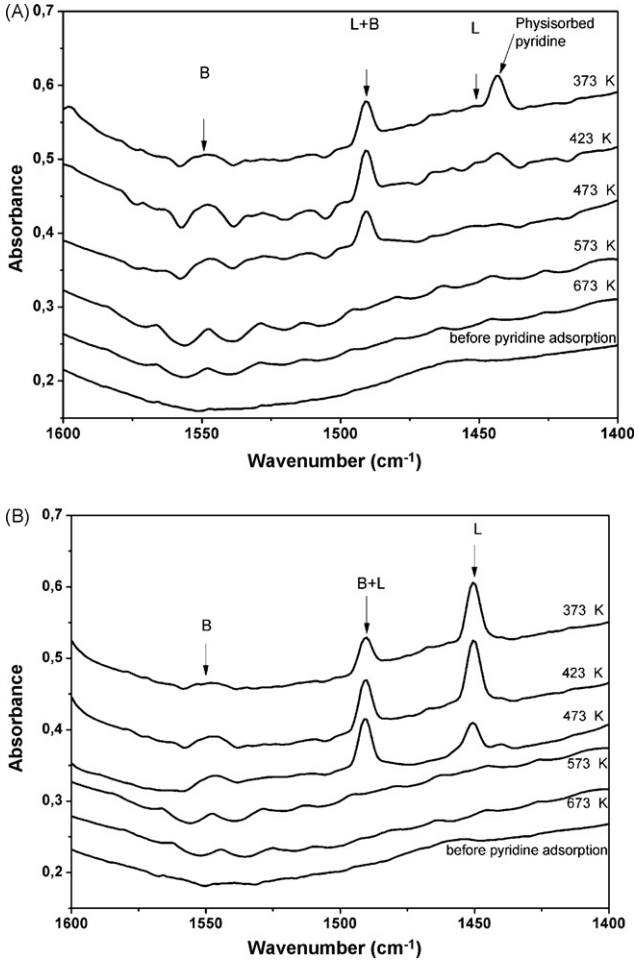

Fig. 3. FTIR spectra of (A) Na-ZSM-12; (B) Ag-ZSM-12, before and after pyridine chemisorption at different temperatures (B and L denote Brönstead and Lewis sites, respectively).

be coherent with peak 1 being ascribed to Lewis acid sites (presumably Na^+ cations), whereas peaks 2 and 3 could be related to Brönsted acid sites of different acid strengths. The density of both Brönsted sites would thus increase by increasing Si/Fe ratio. This suggests that the $Na^+ \leftrightarrow H^+$ exchange equilibrium is displaced toward a higher surface H^+ density with the change in acid strength associated with the decreased density of lattice iron. Again all the above conclusions are coherent with the increase in $C_{Brönsted}/C_{Lewis}$ ratios reported in Table 4.

The observed desorption temperatures and desorbed NH_3 amounts in Al-Fe ZSM-12 samples are found to be intermediate values of Al-ZSM-12 and Fe-ZSM-12 results.

4.7. Temperature-programmed desorption

4.7.1. Binary toluene–ethylene mixture

Representative TPD profiles obtained over selected samples are presented in Fig. 5 and the results are summarized in Table 6. Several factors, such as mode of metal substitution, acid properties, framework or extra-framework species in the pore lattice, extent of metal substitution and/or distribution have to be considered to understand the observed trapping capacities and profiles [19]. It can be observed from these results that the desorption profiles of ethylene and toluene are homothetic, compatible with the single-file diffusion mechanism, since the smaller, less-strongly adsorbed molecule (ethylene) is desorbed simultaneously with the larger,

Table 5
NH_3-TPD results

Sample	T_{peak1} (°C)	NH_3 (mol/g cat × 10^5)	NH_3 (mol/m^2 × 10^7)	T_{peak2} (°C)	NH_3 (mol/g cat × 10^5)	NH_3 (mol/m^2 × 10^7)	T_{peak3} (°C)	NH_3 (mol/g cat × 10^5)	NH_3 (mol/m^2 × 10^7)
Na-ZSM-12	160	2.9	0.8	212	27.4	8.0	395	190.9	55.8
H-ZSM-12	143	24.3	7.5	310	70.2	21.7	380	218.1	67.3
Ag-ZSM-12	200	34.5	11.8	263	9.5	32.4	375	70.3	24.0
Mg-ZSM-12	118	10.2	4.0	141	21.9	8.5	193	30.1	11.7
Fe-ZSM-12 (40)	117	37.7	18.5	175	8.3	4.2	230	11.9	4.2
Fe-ZSM-12 (50)	133	10.8	3.7	175	13.8	4.7	242	15.7	5.4
Fe-ZSM-12 (70)	145	5.1	1.6	175	15.1	4.9	245	17.3	5.6
Al-Fe-ZSM-12 (40)	143	20.6	6.1	205	47.8	14.1	320	34.2	1.0
Al-Fe-ZSM-12 (60)	173	19.2	8.2	220	30.1	12.8	320	54.6	23.3

Table 6
Toluene–ethylene binary TPD results

Sample* (trivalent element)	Desorbed amounts (mmol/g)		Molar ratio Toluene/ethylene	Desorption temperature (°C)	
	Ethylene	Toluene		Ethylene	Toluene
Na-ZSM-12 (Al)	0.104	0.778	7.5	138, 282	138, 282
H-ZSM-12 (Al)	0.045	1.001	22.2	130, 215	142, 183
Ag-ZSM-12 (Al)	0.108	0.626	5.8	125	150, 311
Mg-ZSM-12 (Al)	0.069	0.340	4.9	148	153, 248
Na-ZSM-12 (Fe, 40)	0.037	0.388	10.5	113	147, 262
Na-ZSM-12 (Fe, 50)	0.042	0.440	10.5	147	149, 270
Na-ZSM-12 (Fe, 70)	0.047	0.559	11.9	161	160, 284
Na-ZSM-12 (Al, Fe, 40)	0.045	0.551	12.2	122	140, 272
Na-ZSM-12 (Al, Fe, 60)	0.029	0.339	11.7	152	157, 276

* The samples have MTW structure with 12R aperture, pore diameter 5.6 × 6.0 Å and non-intersecting 1D pore lattice.

more-strongly adsorbed one (toluene) [19,22]. For all the toluene profiles, there are two desorption peaks, as shown in Fig. 5. The high temperature peak is more important in the case of Na-ZSM-12 (Fig. 5A) than in the other samples, which could be attributed to stronger interactions of toluene with the strong Brönsted acid sites present in this sample. A dominant desorption peak is observed for ethylene in the temperature range 113–161 °C in all samples, except in the cases of Na and H-ZSM-12. These materials exhibit two desorption peaks, the second ones being observed at 282 and 215 °C, respectively. The main desorption peak of ethylene in the temperature range of 113–161 °C is similar to the first desorption peak of toluene in the range of 138–160 °C, particularly in the case of Fe samples (Fig. 5D). The second high temperature desorption peak of toluene, over the temperature range of 183–311 °C, can be attributed to specific strong interaction of toluene molecules with stronger acid sites.

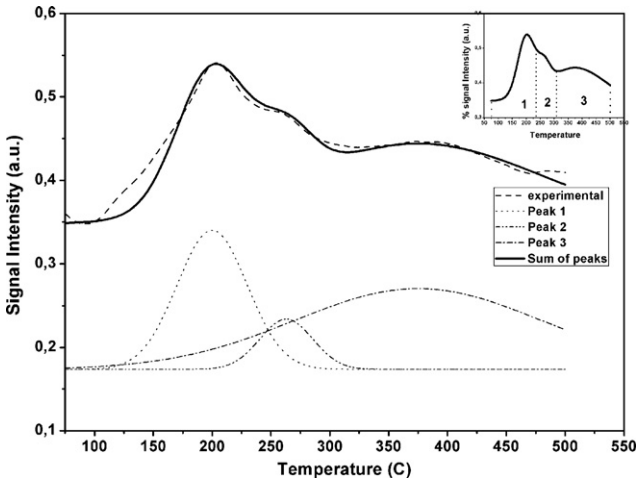

Fig. 4. Ammonia thermodesorption profile of Ag-ZSM-12.

In the case of Ag-ZSM-12, the high desorption temperature of the second peak reaches up to 300 °C due to strong interactions between toluene and Ag trapping centres. Thus, this hydrocarbon can be retained up to temperatures well above the light-off temperature of the catalytic muffler.

As noted above the second toluene peak is most pronounced for Na-ZSM-12 sample (Fig. 5 A), around 282 °C, which is also well above the light-off temperature of the muffler catalyst.

It can be noticed that a clear relation exists between desorption temperature and the degree of substitution of Fe^{3+} in iron substituted samples. By decreasing the amount of Fe^{3+} in these samples, the desorption temperatures of both ethylene and toluene increase due to appearance of progressively stronger Brönsted acid sites (Table 6). For instance, the higher desorption peak of toluene in the case of Si/Fe = 70 reaches 284 °C.

The total numbers of moles of ethylene and toluene desorbed were converted into adsorbed volumes assuming molar volumes of 0.105 and 0.075 ml/mmol for toluene and ethylene, respectively. The sums of these values are estimates of total sorbate volume. They are plotted against micropore volume in Fig. 6 in a same manner as in ref. [19]. The curve shown in Fig. 6 was established from our previous studies of about 30 different zeolites and AlPOs. It is reported here for the sake of a global comparison with these previous data.

All the samples have micropore volume > 0.10 ml/g. The micropore volume values on this graph are close to each other since all samples have the same MTW structure. It is clear that H-ZSM-12 has the highest adsorption capacity among these samples and this capacity decreases in the order: $H^+ > Na^+ > Ag^+ > Mg^{2+}$ for Al based ZSM-12. It is obvious from Fig. 6 that by increasing the Si/Fe ratio in the samples, the adsorption capacity is also increased. This is due to the creation of stronger acid sites, as established by FTIR results of adsorbed pyridine and thermodesorption of ammonia, and as discussed in the previous section.

Two samples Al-Fe-ZSM-12 (60) and Al-ZSM-12 (Mg) have low adsorption capacities probably due to extra-framework oxidic

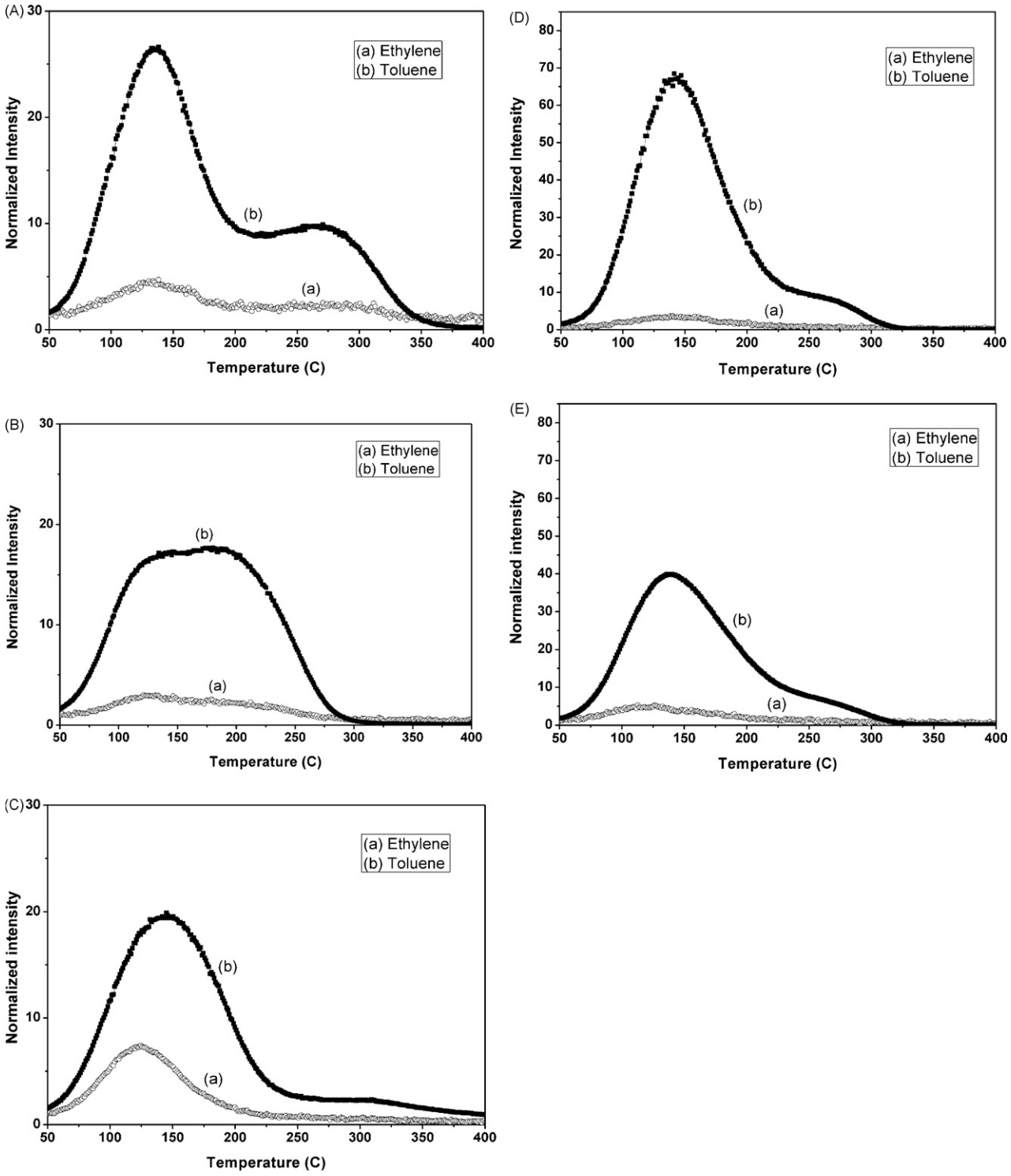

Fig. 5. Toluene/ethylene binary mixture TPD profiles of selected as-synthesized samples. (A) Na-ZSM-12; (B) H-ZSM-12; (C) Ag-ZSM-12; (D) Fe-ZSM-12 (70); (E) Al-FZSM-12 (40).

material that causes pore blocking and reduces the trapping capacity of the sorbates. In fact, the various sorbates used in this work may not access the same pores, so that the micropore volume determined from nitrogen physisorption may not be entirely accessible to the hydrocarbon probes used in this study.

The molar ratio of adsorbed toluene/ethylene is reported in Table 6. The Al-ZSM-12 samples, except for the one in H^+ form, display low values of this ratio in the range of 5–7.5. For instance in the case of Ag-ZSM-12, only one ethylene molecule is trapped by 6 toluene molecules in its micropores. The small relative content of ethylene compared to toluene is indeed surprising since ethylene should diffuse faster within the micropore structure. This result is likely associated with the pore aperture diameter of ZSM-12 (5.6×6.0 Å) which might be too large to be completely obstructed by the toluene molecule. Thus the penetration of toluene might force the ethylene molecules out

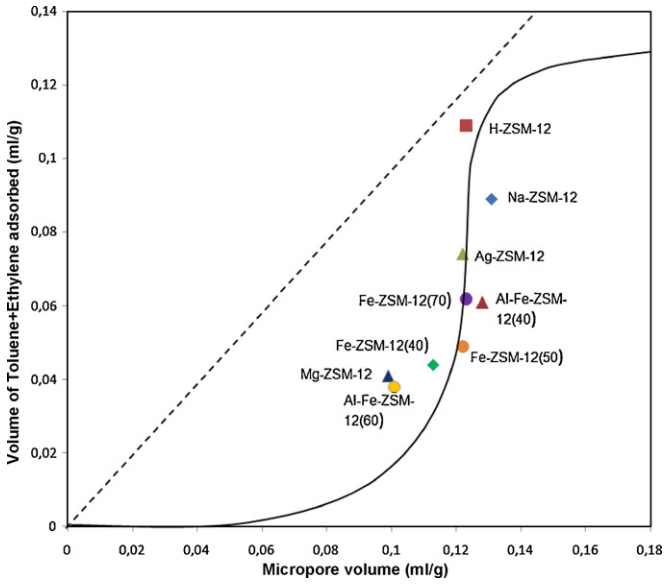

Fig. 6. Volume of the binary (ethylene + toluene) adsorbed phase as a function of micropore volume.

of the pore lattice, making the single-file diffusion process less efficient. For iron substituted samples this ratio varies in the range of 10.5–12.2 indicating that in these cases the amount of ethylene trapped per molecule of toluene is even lower. This can be explained by the effect of isomorphous substitution of Fe^{3+} into the framework of zeolites, which leads to modification in morphology and pore expansion. Indeed introducing a Fe–O bond (1.84 Å) in place of a Al–O bond (1.73 Å) should slightly enlarge the pore aperture and therefore make the single-file diffusion even less efficient.

Besides toluene and ethylene, which are representative of aromatic and olefin components in automobile exhaust, other components such as H_2O and CO_2 are present in high concentrations. It is thus reasonable to collect, investigate and compare the TPD profiles of the samples loaded in different mixture conditions: binary toluene/ethylene mixture, ternary toluene/ethylene/CO_2 mixture, ternary toluene/ethylene/H_2O mixture and quaternary toluene/ethylene/CO_2/H_2O mixture. The TPD profiles and the results of desorption temperature and adsorption capacities of the samples in the case of binary adsorption are presented in Fig. 5 and Table 6. For the other cases, the results are summarized in Fig. 7 and discussed below.

4.7.2. Ternary toluene–ethylene–CO_2 mixture

From the TPD profiles of all samples in the presence of CO_2, it has been found that the adsorption capacities of both ethylene and toluene decrease. This reduction in trapping capacities is explained by the competitive adsorption of CO_2 molecules, which can occupy a portion of hydrocarbon trapping sites. This relative decline in adsorption capacities of both probe molecules is remarkably lower in the case of Ag-ZSM-12.

These differences in sensitivity to CO_2 suggest that adsorption sites of different nature and/or different energetics of adsorption are implemented in these materials. CO_2 is believed to interact with bases. In zeolites the negatively charged oxygen neighbouring the cation is considered a basic site [24]. A stronger Lewis acid, such as the ones observed by NH_3 TPD in Ag-ZSM-12, corresponds to a weaker base, thus explaining the minor variation in adsorption capacity upon adsorption of CO_2 observed for toluene and ethylene in this solid.

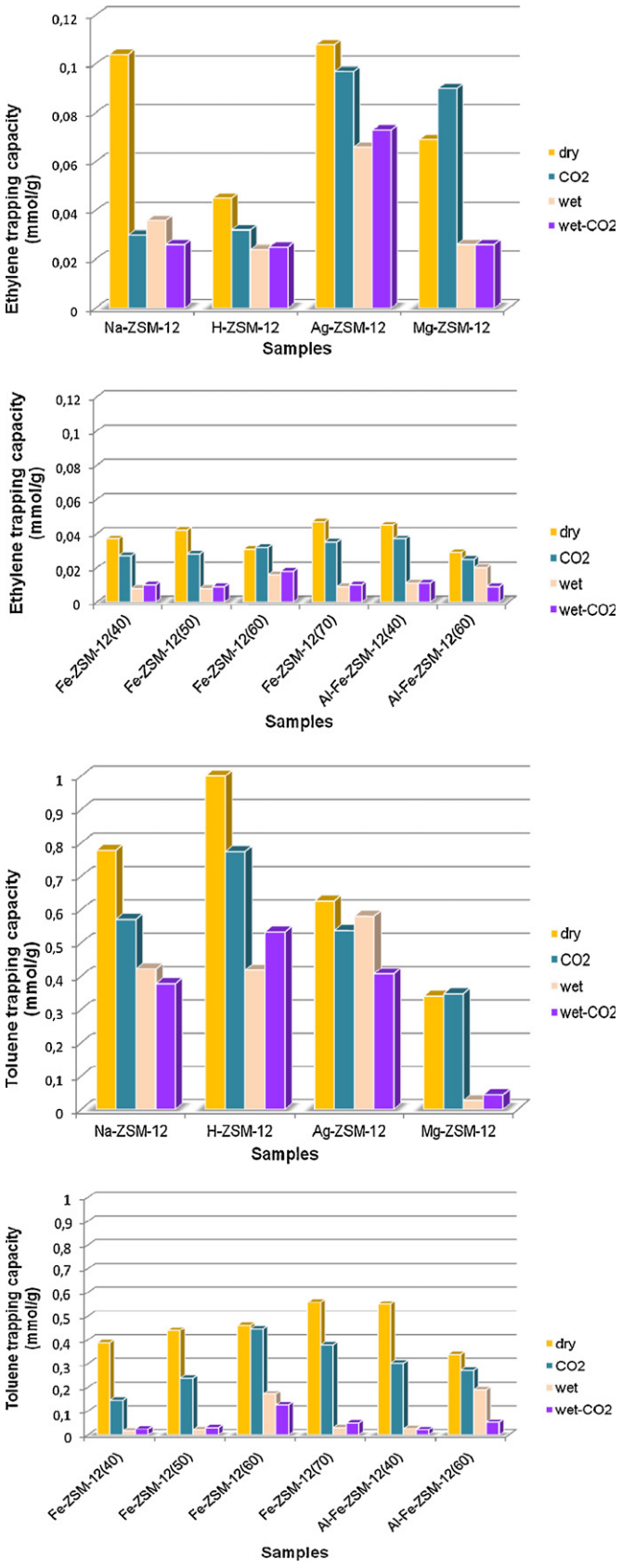

Fig. 7. Comparison of trapping capacities of ethylene/toluene in gas mixtures at different conditions: binary: dry; ternary with CO_2: CO_2; ternary with H_2O: wet; quaternary: wet-CO_2.

In the case of Fe-ZSM-12 it is seen from Fig. 7 that in binary ethylene/toluene adsorption both ethylene and toluene adsorption capacities increase at increasing Si/Fe ratio. Thus, the comparison with NH_3 TPD data (Table 5) suggests that in this case the two hydrocarbons are predominantly adsorbed on Brönsted acid sites. The competitive adsorption effect of CO_2 seems however to decrease at increasing Si/Fe. This in turn suggests competitive adsorption of CO_2 on the ensemble of the Lewis acid and conjugated lattice base. Thus, at least in this case, both Brönsted and Lewis acids constitute adsorption sites for the two hydrocarbons.

4.7.3. Ternary toluene–ethylene–H_2O mixture

The same trend of reduction in adsorption capacities of both sorbates has been obtained for all samples in the presence of H_2O. This reduction is even larger than in the presence of CO_2. Here again, a smaller reduction in toluene and ethylene capacity was found for Ag-ZSM-12 compared to the other zeolites. Very drastic reduction in both toluene and ethylene capacity was systematically obtained on all Fe-ZSM-12 samples.

4.7.4. Quaternary toluene–ethylene–CO_2–H_2O mixture

This experiment is a close simulation of the conditions prevailing at the exhaust of an automobile engine. From the TPD profiles, it was found that the trapping capacities of all samples in the presence of both CO_2 and H_2O are reduced, but the degree of reduction is again not similar for all samples. The decline in adsorption capacities of both toluene and ethylene in the case of Ag-ZSM-12 is not very significant contrary to H-ZSM-12 and almost all the Fe-ZSM-12 samples.

Indeed the significant competitive adsorption of water results from the fact that both Brönsted and Lewis acid sites can adsorb water. The strong interaction corresponding to hydration of the proton implies a strong water adsorption on Brönsted acid sites. This may be an explanation for the lower sensitivity of hydrocarbon adsorption on Ag-ZSM-12 as discussed above. Indeed the dominant hydrocarbon adsorption site would be the Lewis acid in this solid.

5. Conclusion

A systematic study of 12R microporous zeolites with 1D channel lattice as hydrocarbon trap adsorbents for ethylene/toluene under the four conditions of binary, ternary (CO_2 or H_2O) and quaternary mixture in presence of both H_2O and CO_2 has been performed. These one-dimensional zeolites have the same MTW structure but they are differing in some parameters such as: trivalent element (M = Al or/and Fe), Si/M ratio in their lattice, and the nature of cations employed for synthesis and ion-exchange (Na, H, Ag and Mg). The role of these factors in modifying the properties of microporous zeolites acting as adsorbents for reducing the cold-start emissions of automobiles has been investigated.

The single-file diffusion mechanism operated more efficiently in the microporous channels of the Al-ZSM-12 samples, except for Al-ZSM-12 (H) compared to Fe-ZSM-12 samples.

It was moreover found that Fe-ZSM-12 samples were not effective adsorbents for trapping ethylene/toluene owing to their low rate of hydrocarbon adsorption. Their ethylene and toluene adsorption capacities and desorption temperature were not found to be high enough for trapping these hydrocarbons efficiently during the few minutes of the heating time of the exhaust gases during automotive cold-start. Moreover, their adsorption capacity decreases considerably in the presence of H_2O and/or CO_2.

It was shown that Al-ZSM-12 samples possess higher adsorption capacities and desorption temperatures for both ethylene and toluene. In this case, Na-ZSM-12 demonstrates a desorption temperature around 282 °C for both ethylene and toluene due to its strong Brönsted acid sites that create effective interactions with the probe molecules. In the presence of CO_2 and/or H_2O, the adsorption capacity of Al-ZSM-12 samples is reduced but not to such large extent as in the case of Fe-ZSM-12.

On the other hand, Ag-ZSM-12 sample showed an unexpected behaviour under all conditions of TPD experiments. The adsorption capacities of both ethylene and toluene were not significantly changed and showed to be relatively insensitive to the presence of CO_2 and H_2O. In this case desorption temperatures of around 311 and 400 °C for toluene were indeed reached in TPD tests for binary mixture of hydrocarbons and quaternary mixture of hydrocarbons, respectively. These results were explained by the dominating role of strong Lewis acid sites present in this adsorbent. Consequently, this solid could be considered as a promising adsorbent for controlling cold-start emissions.

Acknowledgement

The authors gratefully acknowledge Natural Sciences and Engineering Research Council of Canada (NSERC) for providing financial support for this study.

Appendix A. Supplementary data

Supplementary data associated with this article can be found, in the online version, at doi:10.1016/j.apcatb.2008.08.025.

References

[1] T. Kirchner, A. Donnerstag, A. Koenig, G. Eigenberger, in: N. Cruse, A. Frennet, J.M. Bastin (Eds.), 4th International Congress on Catalysis and Automotive Pollution Control, 1997, p. 39.
[2] J.E. Kubsh, SAE Paper 941996, 1994.
[3] K.P. Reddy, S.T. Gulati, D.W. Lambert, P.S. Schmidt, D.S. Weiss, SAE Paper 940782, 1994.
[4] H. Mizuno, F. Abe, S. Hashimoto, T. Kondo, SAE Paper 940466, 1994.
[5] P.F. Kuper, W. Maus, H. Swars, R. Bruck, F.W. Kaiser, SAE Paper, 940465, 1994.
[6] N.R. Collins, G.R. Chandler, R.J. Brisley, P.J. Andersen, P.J. Shady, S.A. Roth, SAE Paper 960799, 1996.
[7] B. Pfalzgraf, M. Rieger, G. Ottowitz, SAE Paper 960261, 1996.
[8] T. Ma, N. Collings, T. Hands, SAE Paper, 920400, 1992.
[9] T. Tsoi-Hei Ma, UK patent application GB 2280128 A, 1995.
[10] S.P. Elangovan, M. Ogura, S. Ernst, M. Hartmann, S. Tontisirin, M.E. Davis, T. Okubo, Micropor. Mesopor. Mater. 96 (2006) 210–215.
[11] D.S. Lafyatis, G.P. Ansell, S.C. Bennett, J.C. Frost, P.J. Millington, R.R. Rajaram, A.P. Walker, T.H. Ballinger, Appl. Catal. B–Environ. 18 (1998) 123–135.
[12] R.M. Heck, R.J. Farrauto, Appl. Catal. A–Gen. 221 (2001) 443–457.
[13] B. Bigot, V.H. Peuch, J. Phys. Chem. B 102 (1998) 8696–8703.
[14] S.P. Elangovan, M. Ogura, Y. Zhang, N. Chino, T. Okubo, Appl. Catal. B–Environ. 57 (2005) 31–36.
[15] N.R. Burke, D.L. Trimm, R. Howe, N.W. Cant, in: I.E. Aust (Ed.), Proceedings of the CHEMECA 98 Conference, Port Douglas, Paper No. 87, 1998.
[16] N.R. Bruke, D.L. Trimm, R.F. Howe, Appl. Catal. B–Environ. 46 (2003) 97–104.
[17] S.P. Elangovan, M. Ogura, M.E. Davis, T. Okubo, J. Phys. Chem. B 108 (2004) 13059.
[18] K.F. Czaplewski, T.L. Reitz, Y.J. Kim, R.Q. Snurr, Micropor. Mesopor. Mater. 56 (2002) 55–64.
[19] A. Iliyas, Z. Sarshar, M.H. Zahedi-Niaki, M. Eić, S. Kaliaguine, submitted for publication.
[20] S. Ernst, P.A. Jacobs, J.A. Martens, J. Weitkamp, Zeolites 7 (1997) 458–462.
[21] P. Ratnasamy, R. Kumar, Catal. Today 9 (1991) 329–416.
[22] A. Iliyas, M.H. Zahedi-Niaki, M. Eic, S. Kaliaguine, Micropor. Mesopor. Mater. 102 (2007) 171–177.
[23] J. Pérez-Ramírez, J.C. Groen, A. Brückner, M.S. Kumar, U. Bentrup, M.N. Debbagh, L.A. Villaescusa, J. Catal. 232 (2005) 318–334.
[24] M. Huang, A. Adnot, S. Kaliaguine, J. Catal. 137 (1992) 322–332.